JGR Biogeosciences

RESEARCH ARTICLE
10.1029/2019JG005032

N_2O Emissions From Two Agroecosystems: High Spatial Variability and Long Pulses Observed Using Static Chambers and the Flux-Gradient Technique

Sarah Waldo[1,2], Eric S. Russell[1], Kirill Kostyanovsky[3,4], Shelley N. Pressley[1], Patrick T. O'Keeffe[1], David R. Huggins[5], Claudio O. Stöckle[6], William L. Pan[3], and Brian K. Lamb[1]

[1]Laboratory for Atmospheric Research, Department of Civil and Environmental Engineering, Washington State University, Pullman, WA, USA, [2]National Risk Management Research Laboratory, United States Environmental Protection Agency, Office of Research and Development, Cincinnati, OH, USA, [3]Department of Crop and Soil Sciences, Washington State University, Pullman, WA, USA, [4]Bureau of Environmental Planning and Analysis, New York City Department of Environmental Protection, Flushing, NY, USA, [5]Northwest Sustainable Agroecosystems Research Unit, USDA-ARS, Washington State University, Pullman, WA, USA, [6]Department of Biological and Agricultural Engineering, Washington State University, Pullman, WA, USA

Key Points:
- Total emissions from 1 April to 30 September 2015 were 2.4 ± 0.7 and 2.1 ± 0.2 kg N_2O-N/ha at the no- and conventional-till sites, respectively
- N_2O fluxes had similar responses to temperature and precipitation at both sites
- High spatial variability at both sites (CVs > 140%) limited the ability of the chamber systems to characterize field-scale N_2O emissions

Supporting Information:
- Supporting Information S1

Correspondence to:
S. Waldo,
waldo.sarah@epa.gov

Citation:
Waldo, S., Russell, E. S., Kostyanovsky, K., Pressley, S. N., O'Keeffe, P. T., Huggins, D. R., et al. (2019). N_2O emissions from two agroecosystems: High spatial variability and long pulses observed using static chambers and the flux-gradient technique. *Journal of Geophysical Research: Biogeosciences*, *124*, 1887–1904. https://doi.org/10.1029/2019JG005032

Received 17 JAN 2019
Accepted 6 JUN 2019
Accepted article online 22 JUN 2019
Published online 6 JUL 2019

Abstract With the addition of nitrogen (N), agricultural soils are the main anthropogenic source of N_2O, but high spatial and temporal variabilities make N_2O emissions difficult to characterize at the field scale. This study used flux-gradient measurements to continuously monitor N_2O emissions at two agricultural fields under different management regimes in the inland Pacific Northwest of Washington State, USA. Automated 16-chamber arrays were also deployed at each site; chamber monitoring results aided the interpretation of the flux gradient results. The cumulative emissions over the six-month (1 April–30 September) monitoring period were 2.4 ± 0.7 and 2.1 ± 2 kg N_2O-N/ha at the no-till and conventional till sites, respectively. At both sites, maximum N_2O emissions occurred following the first rainfall event after N fertilization, and both sites had monthlong emission pulses. The no-till site had a larger N_2O emission factor than the Intergovernmental Panel on Climate Change Tier 1 emission factor of 1% of the N input, while the conventional-till site's emission factor was close to 1% of the N input. However, these emission factors are likely conservative. We estimate that the global warming potential of the N_2O emissions at these sites is larger than that of the no-till conversion carbon uptake. We recommend the use of chambers to investigate spatiotemporal controls as a complementary method to micrometeorological monitoring, especially in systems with high variability. Continued monitoring coupled with the use of models is necessary to investigate how changing management and environmental conditions will affect N_2O emissions.

Plain Language Summary Nitrous oxide (N_2O) is a greenhouse gas and stratospheric ozone depleting substance that is emitted by soils. Agricultural soils tend to emit more N_2O than natural soils due to the addition of nitrogen fertilizers. N_2O emissions are not well understood on the scale of individual farms, as emissions are difficult to measure at this resolution because they are irregular over time and space. This variability is due to the dependence of N_2O production and emission on soil properties, that is, moisture, nitrogen, and the microbiome. In this study we monitored N_2O emissions from two agricultural fields under different tillage regimes using two complementary methods: the flux-gradient technique and automated chambers. The flux-gradient technique measures N_2O emissions at the field scale, which is relevant to agronomic management. Using both techniques together improves confidence in our results, which give us information on total N_2O emissions from these fields, as well as the relationships between N_2O emissions and rainfall, temperature, and carbon dioxide respiration.

1. Introduction

Nitrous oxide (N_2O) has multiple negative environmental impacts, yet factors affecting N_2O emissions are inadequately understood and difficult to control (Butterbach-Bahl et al., 2013; Galloway et al., 2008; Groffman et al., 2000; Groffman et al., 2006). N_2O is a potent greenhouse gas (GHG), with 265 times the global warming potential of carbon dioxide (CO_2) over a 100-year time horizon (Myhre et al., 2013). Following the phase out of chlorofluorocarbons, N_2O has become the dominant stratospheric ozone-depleting

substance (Ravishankara et al., 2009). N_2O is produced in both natural and managed soils as a by-product of microbial processes, but manure management and the addition of fertilizer nitrogen (N) to agricultural soils elevates N_2O production and emission in agroecosystems. In the United States, it is estimated that agricultural soil management accounts for 77% of anthropogenic N_2O (USEPA, 2017).

Although top-down and bottom-up global estimates of N_2O agree well, there is uncertainty in emission rates at regional and smaller scales (Reay et al., 2012; Syakila & Kroeze, 2012). Reay et al. (2012) call for more measurements of N_2O distributed over major agricultural systems globally to improve local emission estimates and aid in the development of mitigation strategies. Butterbach-Bahl et al. (2013) also emphasized the need for improved measurements to inform agroecological management questions, such as the potential trade-off between soil carbon sequestration and N_2O emissions (Lugato et al., 2018). Agricultural N_2O emissions can increase exponentially with increasing fertilizer application rates (Millar et al., 2018; Shcherbak et al., 2014), highlighting the need for site-specific research over linear emission factors such as those used in the Intergovernmental Panel for Climate Change's (IPCC) methodologies (IPCC, 2006).

Accurate measurements of N_2O emissions are difficult to make because of the high degree of spatial and temporal variability in emissions, or "hot spots" and "hot moments" (Mason et al., 2017; McClain et al., 2003; Molodovskaya et al., 2012; Nicolini et al., 2013). Static chambers (SC) have been used for decades to measure emissions of N_2O from soils; more recently the use of automated multichamber systems has enabled a high degree of temporal coverage relative to manual chambers, but coverage of spatial heterogeneity can still be inadequate (Barton et al., 2015; Butterbach-Bahl et al., 2013; Loescher et al., 2006). Micrometeorological techniques (MM) have high temporal resolution and integrate flux measurements over the field scale (hundreds of square meters, depending on boundary layer turbulence conditions). Furthermore, MM techniques do not disturb the soil and are nondestructive to site vegetation. However, MM requires site conditions to meet strict theoretical assumptions, require a sensitive, stable N_2O instrument with a fast response time, and have demanding power requirements.

How to optimize the use of manual or automated SC and MM for monitoring N_2O emissions is a topic of ongoing discussion in the literature (cf.Bai et al., 2019 ; Jones et al., 2011 ; Nicolini et al., 2013 ; Tallec et al., 2019). Nicolini et al. (2013) point out the mixed results reported in N_2O MM and SC method comparison studies. Careful placement of chambers to be within the micrometeorological flux footprint and be representative of the field-scale spatial variability have been recommended by several studies (e.g., Laville et al., 1999; Loescher et al., 2006; Pihlatie et al., 2005). Advanced SC upscaling techniques such as using footprint analyses and models have resulted in good agreement with MM methods for measuring methane fluxes (Nicolini et al., 2013), and one short-term study of N_2O emissions from sugarcane soils found good agreement between MM results and the mean of the SC measurements (Denmead et al., 2010). However, the drivers of field-scale variability in N_2O emissions, such as inorganic N content, soil moisture, and/or microbial community, are often not readily visible and thus not easy to incorporate into SC deployment or upscaling design in agronomic systems (McDaniel et al., 2017). If the goal of the monitoring is to characterize field-scale emissions, and the field is homogeneous at the macroscale, then in theory the SC location could be independent of the MM flux footprint.

Long-term comparison studies have found limited agreement between the two techniques. This is often attributed the difference to measurement footprints rather than a systematic bias; as discussed in Bai et al. (2019), SC and MM comparison studies show mixed results in terms of total emissions: in some cases, the MM measurements indicate larger emissions than SC (e.g., Bai et al., 2019; Norman et al., 1997; Wang et al., 2013), in other cases the reverse (e.g., Christensen et al., 1996; Neftel et al., 2010; Tallec et al., 2019). Similar to Bai et al. (2019), Jones et al. (2011) attributed the disagreement between their MM and SC results to different coverage of emission hot spots. The authors recommend using the two methods to complement each other: the MM results to monitor overall field-scale N_2O emissions, and SC to interpret the degree of spatial variability and environmental drivers. Similarly, Tallec et al. (2019) highlighted the usefulness of MM results for interpreting the whole-agroecosystem GHG budget and how N_2O emissions respond to environmental drivers at the field scale, and the usefulness of SC results for interpreting soil processes. The authors also list physical disturbance of the site and the need to remove and replace SC to accommodate field management as limits to using SC for defensible annual N_2O emission budgets. These logistical challenges are amplified when monitoring fluxes during spring

thaw, an important N_2O emission hot moment in northern agricultural sites that coincides with challenging field conditions (Flesch et al., 2018).

In this study, we measured fluxes of N_2O from paired agricultural fields in the inland Pacific Northwest United States using both automated static chamber systems and the flux-gradient micrometeorological technique. This intensive monitoring was part of the REgional Approaches to Climate CHange for Pacific Northwest Agriculture project, and sought to address two questions about N_2O emissions and climate mitigation:

1. What are the magnitudes and patterns in N_2O fluxes at these two sites?
2. How do the N_2O fluxes respond to environmental conditions and agronomic management?

The goal of answering these questions is to improve monitoring of N_2O emissions in this region by characterizing key temporal and spatial patterns at these sites. In addition, we critically assess uncertainties in both methods and present recommendations for strategies to investigate N_2O emissions from agricultural fields with high spatial variability.

2. Methods

2.1. Site Description

The two N_2O measurement sites were located <1 km from each other at the Washington State University Cook Agronomy Farm (CAF; 46.78°N, 117.09°W; 800 m above sea level) northeast of Pullman, WA (Figure 1). The region has a semiarid Mediterranean climate with average annual precipitation of 550 mm and an average annual temperature of 9 °C. The average high temperature is 26 °C in the summer and the average winter low is −4 °C. The soils are productive Palouse silt-loam series (fine-silty, mixed, superactive, mesic Pachic Ultic Haploxerolls). Typical springtime soil characteristics at the Cook Agronomy Farm include total soil N of 0.19 ± 0.01%, total C of 2.6 ± 0.1%, and pH of 5.2 ± 0.1 (Shrewsbury et al., 2016). The study site is representative of approximately 0.5 million hectares where dryland annual cropping is practiced in the inland Pacific Northwest (iPNW). The principal management difference between the two sites is the tillage regime. One of the sites was converted to no-tillage management in 1998 (CAF-NT), a practice implemented by ~30% of growers in the iPNW, and the other is managed with conventional reduced tillage (CAF-CT), used by ~40% of growers in the region (Bista et al., 2017). Other management differences include fertilization amount and timing, timing of sowing and harvest, and herbicide application (see Table 1). The N_2O measurement sites were co-located with established eddy covariance flux towers that monitored carbon dioxide, water vapor, and energy fluxes from 2011–2016 and 2012–2016 for CAF-NT and CAF-CT, respectively. Complete descriptions of the eddy covariance systems and auxiliary measurements are in Chi et al. (2016) and Waldo et al. (2016).

The monitoring results presented in this analysis are for the 2015 harvest year, 1 October 2014 to 30 September 2015; both sites were growing spring canola (*Brassica napus*). During the prior year, winter wheat (*Triticum aestivum*) was grown at both sites (Table 1). The winter wheat was harvested in early August 2014 and the residue was retained at both sites, containing 28 ± 3 and 37 ± 6 kg N/ha at CAF-NT and CAF-CT, respectively. CAF-CT was tilled with a chisel plow to a depth of ~0.2 m on 27 October 2014. "Roundup ready" canola was seeded and fertilized on 4 April at CAF-CT, and 18 April at CAF-NT. A combination of anhydrous ammonia and liquid solution N fertilizer was applied at a total rate of 89 kg N/ha at CAF-NT and 100 kg N/ha at CAF-CT. At CAF-NT, the field was seeded and fertilized with a no-tillage drill, while at CAF-CT the fertilizer was deep-banded (~8 cm) with a shank applicator, and simultaneously chisel tilled. Herbicide was sprayed at CAF-NT on 30 May 2015 to terminate weeds in established canola. Both fields were harvested on 14 August 2015, and the canola residue was retained at both sites. Fertilizer was applied at a rate of 168 kg N/ha at CAF-CT on 20 August 2015 for fall planting of winter wheat. Assuming negligible atmospheric N deposition, the total N inputs for the sites as defined by the IPCC emission factor methodology (IPCC, 2006) are equal to the sum of crop residue N and fertilizer N; at CAF-NT this was 115 kg N/ha, and at CAF-CT the total N inputs for the 2015 crop year were 297 kg N/ha. It is arguable whether the N from the 20 August fertilization should be included in the budget; excluding it results in total N inputs of 138 kg N/ha.

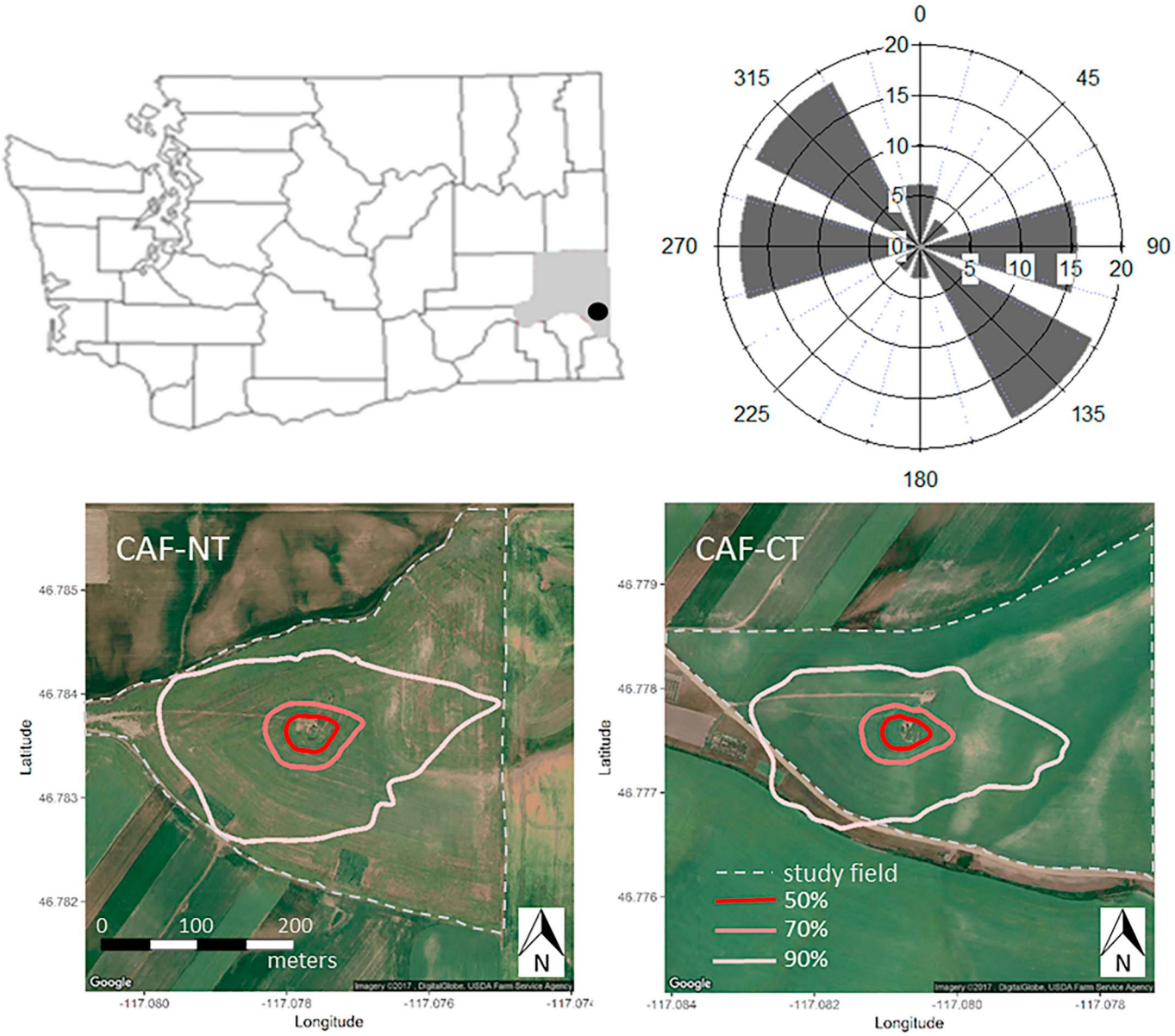

Figure 1. Location and footprint information for the two monitoring sites. The dot in the top left shows the location of the study site in Washington State. The top right wind rose shows the frequency of 45° binned wind directions over the flux-gradient measurement period (April–October 2015). The bottom figures show Google Earth satellite images of the two fields (same scaling). The measurement towers are at the center of the images, the dotted line indicates the extent of the study fields, and the traces indicate 50%, 70%, and 90% of the flux footprint based on the canopy height conditions for 1 April–20 May, encompassing the maximum emission period.

2.2. Flux-Gradient Measurements

The flux-gradient (FG) technique is a micrometeorological technique assuming that turbulent mixing in the atmosphere is analogous to Fick's law of molecular diffusion (Meredith et al., 2014). Fluxes are calculated by multiplying the molar density gradient of a trace gas by the eddy diffusivity, K:

$$F_c = -K \times \frac{\Delta C}{\Delta z} \tag{1}$$

where F_c is the flux of the N_2O (nmol m^{-2} s^{-1}), K is the eddy diffusivity (m^2/s), and ΔC is the gradient of N_2O molar density (nmol/m^3) over Δz, the vertical gradient (m). K is a function of turbulent intensity (Baldocchi

Table 1
Management Activities at the Two Study Sites

Date	CAF-NT	CAF-CT
6 August 2014		Winter wheat harvest, residue ret. (28 kg N/ha)
7 August 2014	Winter wheat harvest, residue ret. (37 kg/ha)	
27 October 2014		Field tilled
4 April 2015		Canola seeded and fertilized (101 kg N/ha)
18 April 2015	Canola seeded and fertilized (87 kg/ha)	
30 May 2015	Herbicide sprayed	
14 August 2015	Canola harvested	Canola harvested
20 August 2015		Fertilized (168 kg N/ha)

et al., 1995; Dunn et al., 2009; Goldstein et al., 1996), and for this study was determined via the modified Bowen ratio technique (Dunn et al., 2009; Liu & Foken, 2001; Meyers et al., 1996). Using temperature as a tracer, K is calculated as

$$K = -\frac{H}{\frac{\Delta T}{\Delta z}\rho_a C_p} \tag{2}$$

where H is the sensible heat flux (W/m^2), ΔT is the difference in temperature (K) at the same heights (Δz, m) as the N_2O measurements, ρ_a is the mass density of air (kg/m^3), and C_p is the specific heat capacity of air (J kg^{-1} K^{-1}). The sensible heat flux was calculated via the eddy covariance technique. The EC fluxes were calculated using EddyPro® version 4.2.0 (LI-COR Biosciences, Lincoln, NE, USA). The H fluxes were gap-filled using the mean diurnal variation method (Falge et al., 2001; Moffat et al., 2007). More details about the EC flux processing and gap-filling the H fluxes at these sites can be found in Waldo et al. (2016) and Chi et al. (2016).

The N_2O mixing ratio was measured at two heights using off-axis integrated cavity output spectroscopy instruments (N_2O/CO 23-d, Los Gatos Research, Mountain View, CA). The gas inlets were installed at heights of 1.2 and 2.5 m above ground level at CAF-CT and 0.8 and 1.9 m at CAF-NT and were outfitted with Teflon particle filters (2 μm). The CAF-NT site had a standard model LGR instrument (part number 907-0014), while at the CAF-CT site the enhanced performance model was used (part number 913-0014); the latter controls the temperature of the optical cell to improve precision and stability of the measurements and has higher power requirements. Temperature was measured at the two heights using aspirated thermistors with a precision of ±0.01 °C (temperature sensor model number: 107-30, aspirated shield model number: 43502-30; both Campbell Scientific, Logan, UT).

The SC and FG systems shared the N_2O instrument on a 4-hr circuit starting at midnight: 3 hr were allocated to cycle through the 16 chambers, and the fourth hour was allocated to the tower. That timeline resulted in six total chamber cycles per day and two 30-min tower fluxes measured 6 times per day (0300, 0330, 0700, 0730, 1100, 1130, 1500, 1530, 1900, 1930, 2300, and 2330). Solenoid valves were used to switch between the measurement systems (Figure S1), and the gradient tubing lines were flushed at a rate of 1.6 L/min by a double-headed bypass pump (B162-AP-AA1 Double Head B-series pump, Air Dimensions Inc., Deerfield Beach, FL, USA). An example of the N_2O and temperature gradient raw time series is shown in Figure S2. More details on the combined SC-FG system can be found in Kostyanovsky et al. (2017).

2.3. Data Filtering, Quality Assurance, and Footprint

The N_2O mixing ratio measurements were filtered for values outside of the plausible range of N_2O ambient mixing ratios (<300 or >400 ppb). The first 60 s after switching from the chamber system to the flux-gradient system were discarded, and the first 16 s of each 60-s gradient height measurement were discarded (Figure S2). Air sample travel time lag was also considered in the calculation. The 30-min average N_2O concentration gradients (ΔC) between the upper (even c_i) and lower (odd c_i) inlet heights were calculated as

$$\Delta C = \frac{1}{n-2} \sum_{i=1,3,5\ldots}^{n-3} c_{i+1} - \frac{c_i + c_{i+2}}{2} + \frac{c_{i+1} + c_{i+3}}{2} - c_{i+2} \quad (3)$$

This averaging procedure puts less weight on the terminal measurements and acts as a high-pass digital filter (Brown & Wagner-Riddle, 2017; Wagner-Riddle et al., 2007).

Zero-gradient tests were performed at each site to quantify any bias in the flux-gradient system. The inlets were co-located at the same height for three days and the resulting "gradient" in N_2O mixing ratios was calculated by taking the mean of the absolute values of the 36 independent data points (Figure S3). We compared the average gradients calculated during these zero-gradient tests to the theoretical minimum detection limit defined by Pattey et al. (2006):

$$\Delta S = \sqrt{\frac{N_h}{n}\ \sigma_s} \quad (4)$$

where $\Delta S_{\min}$ is the resolution of the sampled gradient, N_h is the number of sampling heights, σ_s is the random instrument noise (0.3 ppb on a 1-s basis), and n is the number of samples taken at each level over the sampling period. The nominal value for $\Delta S_{\min}$ is 0.047 ppb N_2O (given $N_h = 2$ sampling heights, n = nominally 270 independent measurements per height over the 30-min sampling period after data filtering, and σ_s of 0.3 ppb). The results of the zero-gradient tests were similar in magnitude to the theoretical minimum detection limit but biased slightly positive. To correct for this bias, the average result from the zero-gradient test at each site was subtracted from the measured gradient before using it to calculate an N_2O flux. Any offset between the aspirated thermistors used to measure the temperature gradient was addressed by calibrating the sensors to each other twice during the measurement period by co-locating the instruments.

The FG N_2O fluxes were filtered for conditions that violate the assumptions of the gradient technique. Periods were discarded if $\Delta T < 0.05$ °C, if the sensible heat flux (H) had the same sign as ΔT, that is, countergradient fluxes, if winds were coming from behind the tower (330–30°), friction velocity (u_*) < 0.13, or if the period was classified as poorest quality based on stationarity and integral turbulence characteristics tests (Foken & Wichura, 1996). Furthermore, we filtered selected 30-min flux periods with random error that exceeded the 97th percentile (fractional error greater than 2,000% and 900% for CAF-NT and CAF-CT, respectively).

The flux contribution footprint for each 30-min FG measurement was determined using the Flux Footprint Prediction model developed by Kljun et al. (2015). The measurement height of the sonic anemometer at each site was used as the reference height (1.91 and 2.21 m at CAF-NT and CAF-CT, respectively). Canopy height, used to determine roughness length and displacement height, was calculated by averaging measurements of crop height taken at four points around the flux tower every two weeks during the growing season.

2.4. Chamber Measurements

An array of 16 static automated chambers (LI-8100, LiCor Biosciences, Lincoln, NE) was installed at each site. The LI-8100 instrumentation has a carbon dioxide (CO_2) analyzer and a multiplexer to control the sample gas flow from the 16 chambers. The chambers were arranged in four parallel lines approximately 20 m apart, with approximately 2 m between each chamber, covering a total grid area of ~360 m^2. The N_2O mixing ratio within the chamber headspace was measured with the same integrated cavity output spectroscopy instruments used to measure N_2O for the flux-gradient system (section 2.2). The N_2O flux out of the soil was calculated as

$$F_{N_2O} = \frac{\Delta N_2O}{\Delta t} \times \frac{V}{A} \quad (5)$$

where $\Delta N_2O/\Delta t$ is the change in N_2O molar density (nmol/m^3) observed in the chamber during each sample period (Δt), determined from a best fit linear or exponential regression of the instrument output versus time during each sampling period; V is the volume (m^3) of the chamber system including tubing and instrument cavities; and A (m^2) is the surface area of the chamber surface. The effective noise level (3σ) of the N_2O

instrument is 0.3 ppb on a 1-s basis which yields a minimum flux detection limit of 0.008 nmol N_2O m^{-2} s^{-1} for the chamber method. The chamber system is described in more detail by Kostyanovsky et al. (2017).

2.5. Uncertainty Parameterization

2.5.1. Random Uncertainty in the Flux Gradient Measurements

Uncertainty in the N_2O fluxes calculated with the flux-gradient technique was determined by propagating the random error associated with each of the component measurements: ΔC, H, ΔT, and Δz. Errors in ρa and Cp were deemed negligible. The random error in the N_2O concentration gradient ($E_{\Delta C}$) was calculated as

$$E_{\Delta C} = \sqrt{\frac{{\sigma_{z_1}}^2}{n_1} + \frac{{\sigma_{z_2}}^2}{n_2}} \tag{6}$$

where σ_{z1} and σ_{z2} are the standard deviations of the N_2O concentration measurements at heights z_1 and z_2, respectively, and n_1 and n_2 are the number of observations at the two heights. The uncertainty in H was parameterized as the variance of the covariance (Finkelstein & Sims, 2001). The random error in the temperature gradient was calculated similar to the N_2O concentration gradient, using the measured standard deviations. Error in the gradient separation height, Δz, due to "droopiness" of the lines after weather events, etc., was estimated to be 5%, or 5–6 cm. The random error of the N_2O flux was calculated by combining the fractional random error of each component source in quadrature and multiplying by the N_2O flux:

$$\mathrm{E_{F_C}} = \sqrt{\left(\frac{\partial \mathrm{F}}{\partial \Delta \mathrm{C}}\mathrm{E_{\Delta C}}\right)^2 + \left(\frac{\partial \mathrm{F}}{\partial \mathrm{H}}\mathrm{E_H}\right)^2 + \left(\frac{\partial \mathrm{F}}{\partial \Delta \mathrm{T}}\mathrm{E_{\Delta T}}\right)^2 + \left(\frac{\partial \mathrm{F}}{\partial_{\Delta z}}\mathrm{E_{\Delta z}}\right)^2} \tag{7}$$

This error was determined for each 30-min flux-gradient measurement period. The 30-min random errors were propagated to daily mean flux random error by summing in quadrature.

2.5.2. Systematic Uncertainty in the Flux Gradient Measurements

To parameterize the systematic uncertainty of the N_2O flux gradient measurements, we looked at two major sources: uncertainty due to one-point sampling (U_{op}) and uncertainty in the eddy diffusivity, K. Previous eddy covariance studies of N_2O fluxes have reported that most of the systematic uncertainty can be attributed to one-point sampling (Kroon et al., 2010; Tallec et al., 2019; Wang et al., 2013). We calculated U_{op} as

$$U_{\mathrm{op}} = \sqrt{\frac{20z}{\mathrm{TU}}}\sqrt[4]{\sigma^2_{\mathrm{N_2O}_{z_1}} + \sigma^2_{\mathrm{N_2O}_{z_2}}} \tag{8}$$

where z is the measurement height (m), T is the averaging time (s), U is the wind speed (m/s), and the ${\sigma^2}_{\mathrm{N2O}}$ terms are the variances in N_2O molar densities measured at each height.

To parameterize the systematic uncertainty in K, we compared the values of K calculated using the modified Bowen ratio technique using temperature as a tracer (equation (2)), with K calculated using similarity theory ("K aerodynamic," hereafter "K_a"; cf. Brown & Wagner-Riddle, 2017):

$$K_a = \frac{\mathrm{u_*}\kappa(\mathrm{z_2}-\mathrm{z_1})}{\ln\left(\frac{\mathrm{z_2}-\mathrm{d}}{\mathrm{z_1}-\mathrm{d}}\right)-\psi_{\mathrm{z_2}}+\psi_{\mathrm{z_1}}} \tag{9}$$

where u_* is the friction velocity, κ is the von Karman constant ($\kappa = 0.40$), z_2 and z_1 are the two gradient measurement heights, d is the zero-plane displacement height, and ψ_{z2} and ψ_{z1} are the integrated Monin-Obukhov similarity functions for heat for each sampling height. The similarity functions depend on stability conditions, categorized by $\zeta = (z - d)\ \mathrm{L}^{-1}$, and can be calculated using the Businger-Dyer relationships (Businger et al., 1971; Dyer & Hicks, 1970):

$$\psi = \begin{cases} 2\ln\left(\frac{1+x^2}{2}\right),\ x = (1-15\zeta)^{\frac{1}{4}} & Unstable, \zeta <= -0.01 \\ -4.7\zeta & Stable, \zeta >= 0.01 \\ 0 & Neutral, -0.01 < \zeta < 0.01 \end{cases} \tag{10}$$

where L is the Monin-Obukhov length:

$$L = \frac{\left(-u_*^3 T_v\right)}{\kappa g \overline{w' T_v'}} \tag{11}$$

where T_v is the virtual temperature, g is the acceleration due to gravity, and $w'T_v'$ is the kinematic virtual temperature flux.

2.5.3. Uncertainty in the Chamber Measurements

The uncertainty in the daily N_2O emissions measured by the chambers was estimated by calculating the 95% confidence interval of the arithmetic mean chamber N_2O emission averaged between individual chambers and over the six daily observation cycles (both space and time). Since neither data set followed a normal, log-normal, or other discernable distribution, we used a nonparametric Chebyshev-type inequality to calculate the 95% confidence interval of each chamber data set (Singh et al., 2006).

2.6. Determining Cumulative N_2O Emissions and Relation of N_2O to CO_2

Cumulative N_2O emissions for both sites and both methods were determined by integrating the daily mean N_2O emissions over the measurement period. Gaps in the daily N_2O emissions time series were filled via linear interpolation. This gap-filling strategy was selected for simplicity. Uncertainties were propagated from daily to cumulative fluxes for both the chamber and flux-gradient results by summing in quadrature. To compare the relative impact of N_2O and CO_2 fluxes in these systems, we converted the N_2O emissions to CO_2-eq using the global warming potential factor of 265 kg N_2O per kg CO_2 (Myhre et al., 2013).

3. Results

3.1. N_2O Monitoring Results

Emissions of N_2O had the same general trend over time at both sites: they increased from baseline levels after canola was planted and fertilized in the spring to peak levels in mid-May, coinciding with a heavy precipitation event that took place from 12 to 16 May 2015 (Figure 2). Maximum daily N_2O emission values measured at CAF-NT by the FG and SC systems were 202 ± 65 and 54 ± 26 g N_2O-N ha^{-1} d^{-1} on 21 and 24 May, respectively. Maximum daily N_2O emission values measured at CAF-CT by the FG and SC methods were 94 ± 48 and 136 ± 67 g N_2O-N ha^{-1} d^{-1} on 14 and 19 May, respectively. N_2O emissions then decreased to a baseline close to zero (<14 g N_2O-N ha^{-1} d^{-1} at CAF-NT and <3.5 g N_2O-N ha^{-1} d^{-1} at CAF-CT) from late June through August, punctuated by a brief spike in N_2O emissions due to a rainfall event on 10 July 2015 (observed in each data set except for the CAF-NT FG measurements). Emissions increased moderately in September, coinciding with rainfall events. The SC results for 1 October 2014 to 1 April 2015 show that both sites had measurable N_2O emissions during the winter; larger N_2O emissions were measured by SC at the CAF-NT site than the CAF-CT site (Figure 2). Most chambers at both sites had a diurnal pattern of elevated afternoon N_2O emissions (Figures S4 and S5). No clear diurnal pattern is discernible in the FG results (Figure S6), but the lack of temporal coverage, especially over the periods of 0700 and 1900, likely contributed to this (Figure S7).

We compared the SC and FG results at the two sites separately for periods of elevated and baseline fluxes (Table 2; cf. Tallec et al., 2019). We defined 15–29 July 2015 as the baseline period and 12–26 May 2015 as the emission pulse period. We used evaporation as a proxy for soil moisture in comparing the two periods at the two sites. Evaporation (E) was parameterized via partitioning the latent heat flux (LE) measured via eddy covariance into evaporation and transpiration (see Chi et al., 2016). The CAF-CT site saw a larger difference in E between the midsummer baseline period and the early summer emission pulse than CAF-NT did. The drop in E at CAF-CT, indicating a drop in soil moisture relative to CAF-NT, is consistent with previous results at these two sites: during the 2013 crop year (both sites growing garbanzo beans) CAF-NT had consistently higher soil water content than CAF-CT at 18- and 30-cm depths. This difference can be attributed to tillage management; no-till management can reduce evaporation and increase precipitation infiltration (Chi et al., 2016; Chi et al., 2017). However, the differences in N_2O emission magnitude between the FG and SC results at both sites make it difficult to interpret the impact of field-scale soil moisture effects on N_2O

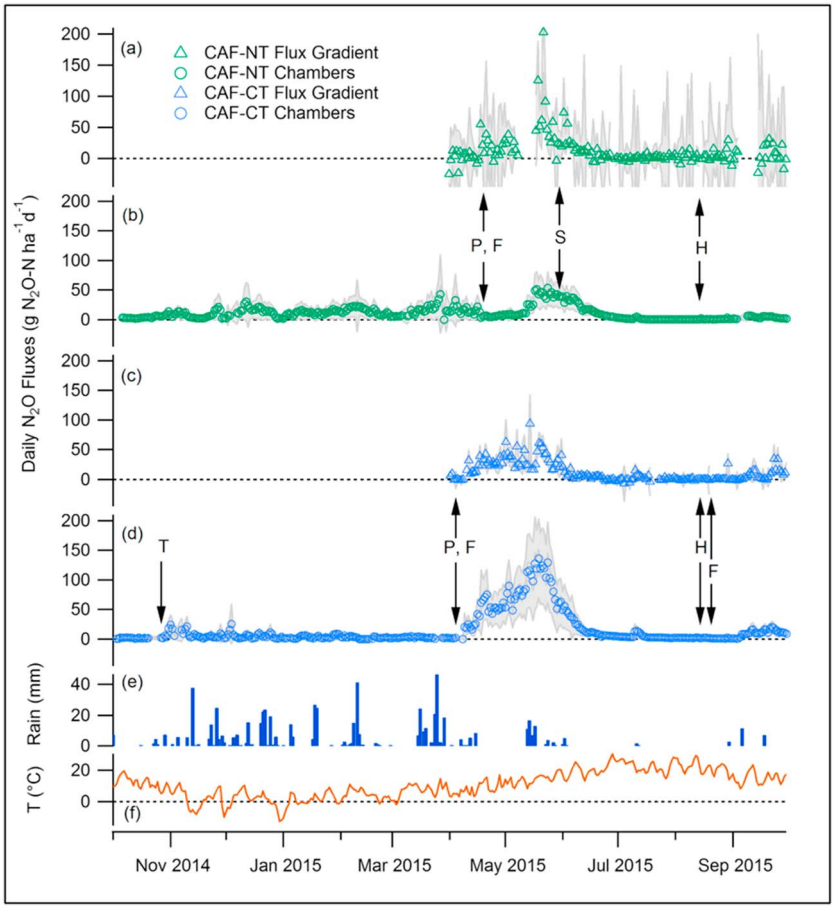

Figure 2. Time series of N_2O fluxes. (a) CAF-NT FG, (b) CAF-NT chambers, (c) CAF-CT FG, and (d) CAF-CT chambers. (e) Precipitation and (f) temperature for the 2015 crop year. Management activities are indicated by T = tillage, planting, F = fertilization, S = herbicide spray application, and H = harvest.

Table 2

Summary Statistics (Mean, Coefficient of Variation (CV), Number of Independent Observations (N), and Lower 5% and Upper 95% Intervals) During a Two-Week Baseline Emission Period (15–29 July 2015) and During Two Weeks of the Emission Pulsed (12–26 May 2015) at Both the No-Tillage and Conventional Tillage Sites (CAF_NT and CAF-CT, Respectively)

		CAF-NT				CAF-CT			
		FG (ng N_2O-N m^{-2} s^{-1})	SC (ng N_2O-N m^{-2} s^{-1})	E (mm m^{-2} d^{-1})	T_{air} (°C)	FG (ng N_2O-N m^{-2} s^{-1})	SC (ng N_2O-N m^{-2} s^{-1})	E (mm m^{-2} d^{-1})	T_{air} (°C)
Baseline (15–29 July)	Mean	2.00	0.51	1.32	20.0	0.25	2.98	0.69	20.2
	CV	580%	113%	90%	26%	1920%	90%	104%	28%
	N	92	1344	670	670	68	1344	670	670
	5th %	−17.0	0	0.17	12.0	−6.42	0.11	0.03	11.6
	95th %	18.6	1.65	3.64	29.1	8.67	8.12	2.08	30.1
Emission pulse (12–26 May)	Mean	74.1	42.2	1.94	14.6	47.7	133	1.98	14.8
	CV	143%	126%	98%	29%	64%	125%	108%	29%
	N	30	1282	670	594	130	1342	670	462
	5th %	5.95	1.63	0.26	8.39	6.35	3.99	0.03	8.60
	95th %	197	160	5.58	21.4	105	501	6.40	21.6

Statistics are reported for the N_2O fluxes measured with the flux gradient method (FG), and the static chamber systems (SC), for latent heat flux (*LE*), and for air temperature (T_{air}), proxies for soil moisture and temperature.

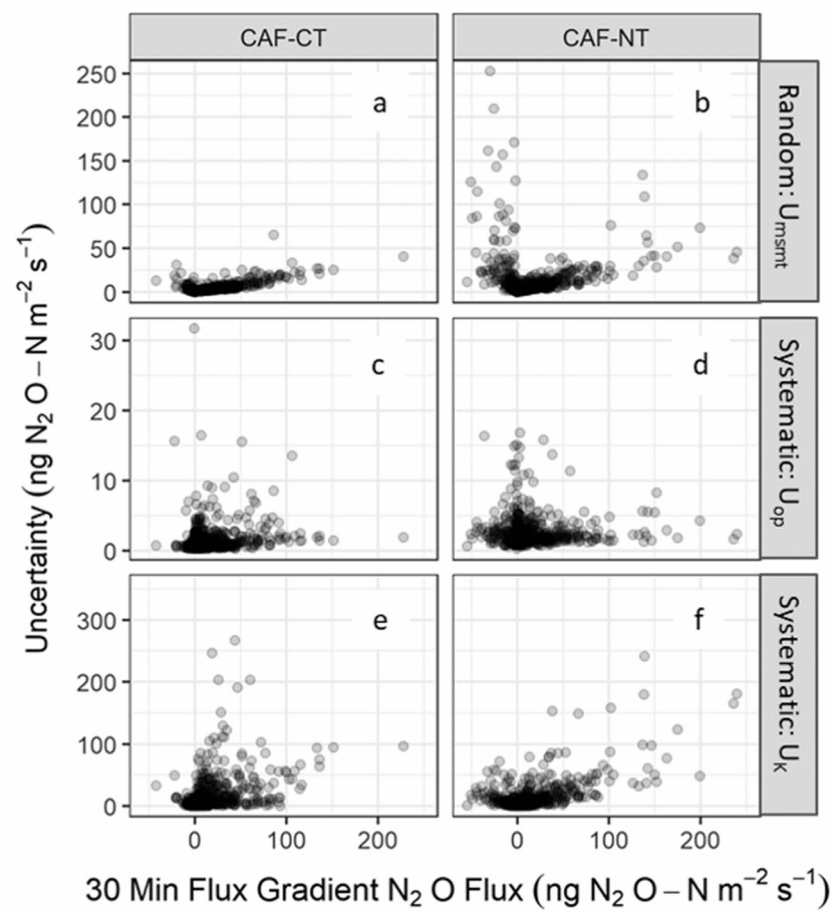

Figure 3. (a and b) Absolute uncertainty due to random measurement error and (c and d) the systematic uncertainties due to one-point sampling and (e and f) assumptions in the parameterization of the eddy diffusivity, *K*. Note the difference in *y* axis scales.

emissions during either period. During the baseline period, it is likely that conditions other than moisture (e.g., substrate availability) affected production and emission of N_2O.

3.2. Measurement Uncertainty

3.2.1. Flux-Gradient Random and Systematic Uncertainties

Random measurement error (E_{FC}) accounted for most of the cumulative error at both sites (Figure 3). Propagating E_{FC} over the six-month monitoring period resulted in ±29% and ±7.6% of the cumulative flux for CAF-NT and CAF-CT, respectively. The latter is comparable to random error magnitudes reported in Brown and Wagner-Riddle (2017), while the former is more similar to the error ranges reported by Phillips et al. (2007). We attribute the difference in random error to the different instruments used: the high-performance instrument at CAF-CT was better able to resolve N_2O gradients and recorded less noise than the instrument at CAF-NT. Random errors in the measurement of the N_2O gradient ($E_{\Delta C}$) was the largest contributor to E_{FC} at both sites: the median contributions of $E_{\Delta C}$ to E_{FC} for all 30-min FG calculation periods were 98% and 91% at CAF-NT and CAF-CT, respectively.

Systematic uncertainty due to one-point sampling was a smaller source of uncertainty than due to characterization of *K* (U_K), the latter of which notably did not follow the same exponential decay in fractional uncertainty with an increase in flux magnitude (Figure S8). We chose not to include the U_K in our overall uncertainty calculation. Due to the nonideal hilly topography of our study locations (Figure S9), we argue that using a tracer is a more direct method of characterizing the eddy diffusivity, violating fewer assumptions than similarity theory does. See Figure S10 for a direct comparison of the two *K* terms. It would be

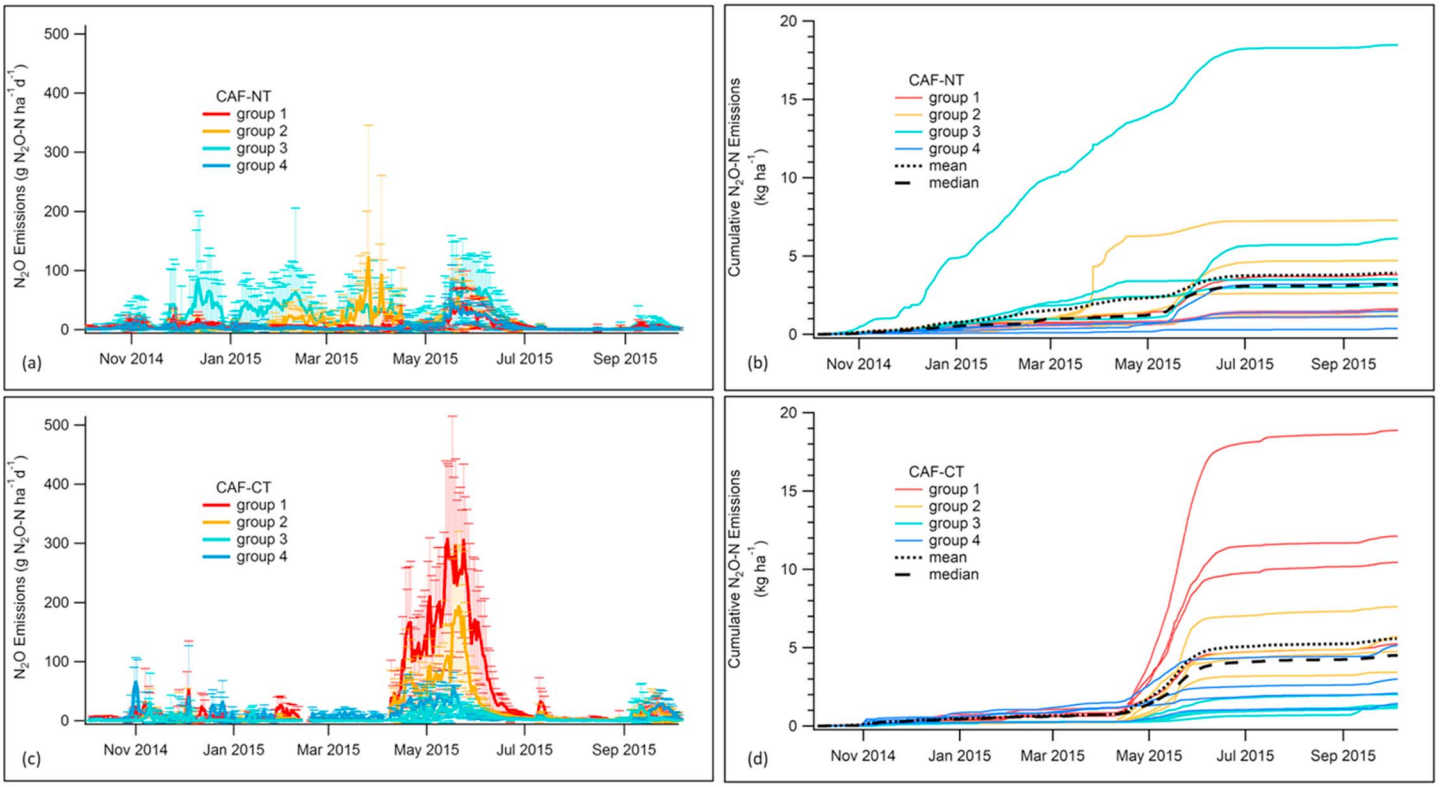

Figure 4. Time series of (a and c) daily and (b and d) cumulative N_2O emissions by chamber group. Whiskers in (a) and (c) indicate 95% confidence interval.

appropriate to include U_K if both the modified Bowen ratio method with temperature as a tracer (K_T) and similarity theory (K_a) were equally well suited for our sites.

The systematic uncertainty due to one-point sampling (U_{op}) was more important to the overall uncertainty of the 30-min N_2O fluxes at CAF-CT than at CAF-NT. The median contributions of fractional U_{op} and random measurement fractional error to the total (sum of random and systematic) error for all 30-min FG calculation periods were 45% and 47%, respectively, at CAF-CT, and 22% and 77%, respectively, at CAF-NT. The U_{op} error had a larger impact on smaller-magnitude fluxes (Figure 3). The propagated U_{op} error of the cumulative fluxes over the six-month monitoring period represented ±0.3% of the cumulative flux for CAF-NT and ±0.6% for CAF-CT, more than an order of magnitude smaller than the cumulative uncertainty from random measurement error.

The results of the FG zero gradient tests indicated slight positive biases at both sites: 0.042 ± 0.022 ppb/m at CAF-NT and 0.021 ± 0.010 ppb/m at CAF-CT (Figure S3). These values are similar in magnitude to the average theoretical minimum detection limits calculated with equation (7) of 0.040 ± 0.006 and 0.032 ± 0.006 ppb/m at CAF-NT and CAF-CT, respectively. The lower level of noise at the CAF-CT site is consistent with the advantages of the enhanced performance model LGR instrument deployed at that site.

3.2.2. Chamber Spatial Variability

At both sites, hot spot chambers had disproportionate impacts on the mean upscaled N_2O emissions. Each ~20-cm-diameter chamber comprised 6.25% (1/16th) of the total SC measurement area. The emissions measured at one Group 3 chamber at CAF-NT comprised 25% of the total N_2O emissions (Figure 4b) at that site, and the two highest-emitting chambers accounted for 33% of total emissions. At CAF-CT, the highest emissions measured by a Group 1 chamber comprised almost 17% of the total emissions at that site (Figure 4d), and the two highest measurement sites accounted for 27% of total emissions. Furthermore, the difference between the mean and median illustrate the non-Gaussian distribution of the SC measurements, an indication of systematic uncertainty. The SC cumulative mean and median at CAF-NT are 3.9 and 3.2 kg N_2O-N ha^{-1} yr^{-1}, respectively, and 5.6 and 4.5 kg N_2O-N ha^{-1} yr^{-1}, respectively, at CAF-CT. While we cannot ignore

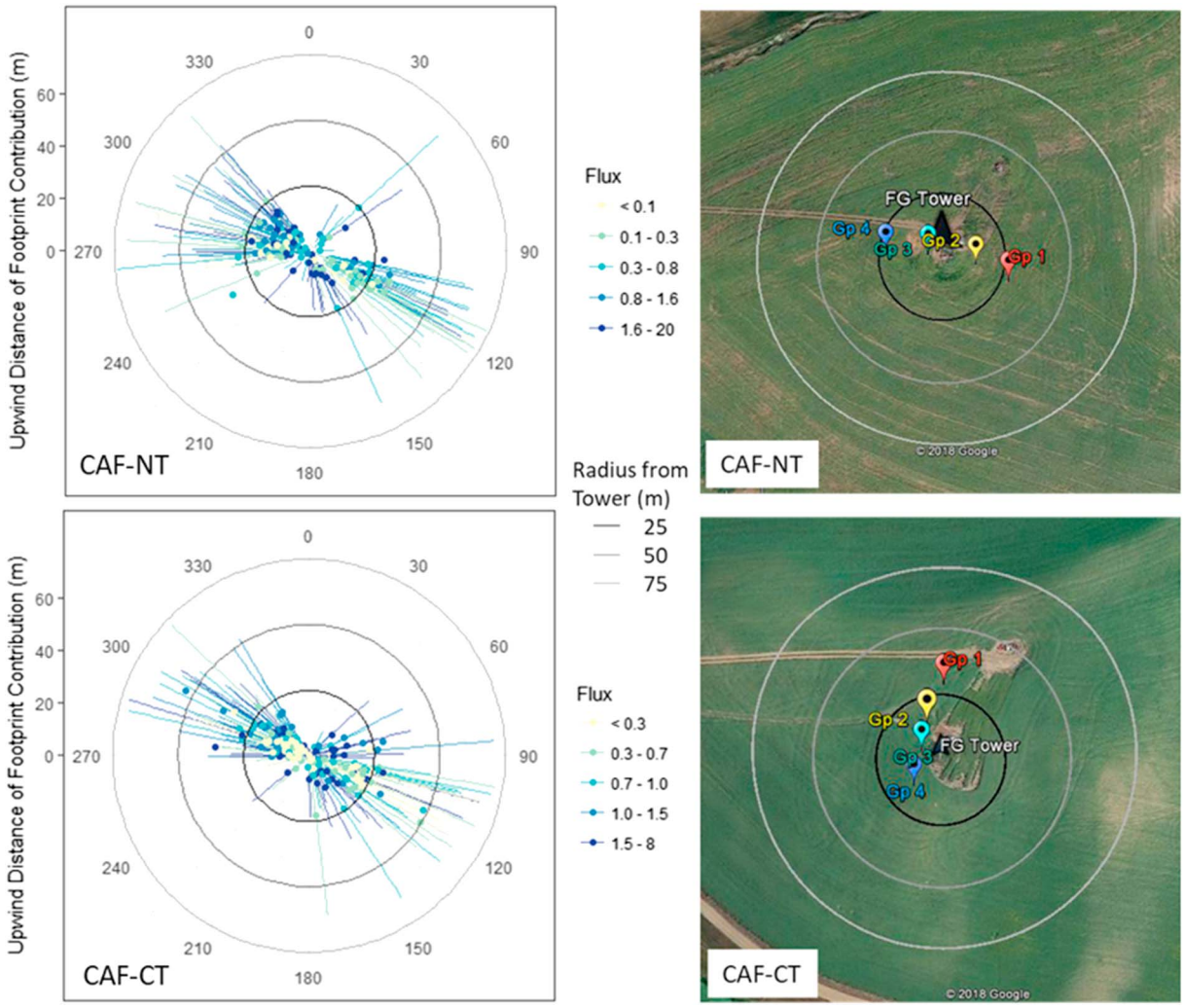

Figure 5. Spatial coverage of (left) flux gradient (FG) and (right) chamber (SC) systems. Rings indicate 25-, 50-, and 75-m radii from the tower. In the FG flux roses, the color of the dots indicates flux magnitude (nmol N_2O m^{-2} s^{-1}), the distance of the dot from the origin the 50% flux contribution extent, and the whiskers the peak and 80% flux contribution extents.

the hot spot chambers, these results highlight the difficulty in characterizing field-scale emissions from SC measurements.

The average spatial coefficient of variation (CV) between 1 October 2014 and 30 September 2015 between all the chambers at CAF-NT was 147%; CAF-CT had a similar average annual CV of 143%. The average CVs during the elevated emission period from 1 April to 1 July 2015 at CAF-NT and CAF-CT were lower than the annual average: 121% and 104%, respectively (Figure S11). The annual average CV values for CO_2 were 96% and 84% for CAF-NT and CAF-CT (not shown). The high CV values indicate that more extensive chamber coverage would be needed to accurately characterize emissions: in a controlled emission study Loescher et al. (2006) found in a system with a CV of 0.8 (the highest CV considered), ≥20 chamber locations were needed to be within 50% of the true mean emission ($\alpha = 0.1$).

3.3. Implications of Spatial Variability on Comparing FG and SC Results

The spatial coverage of the FG and SC systems and their ability to characterize patchy emissions is important when comparing results from the two systems. The soil surface area enclosed by each chamber was ~318 cm^2, for a total measured surface area of 0.51 m^2 at each site. A more liberal way to characterize the SC measurement area is by the dimensions of the area encompassed by the four-chamber by four-chamber grid:

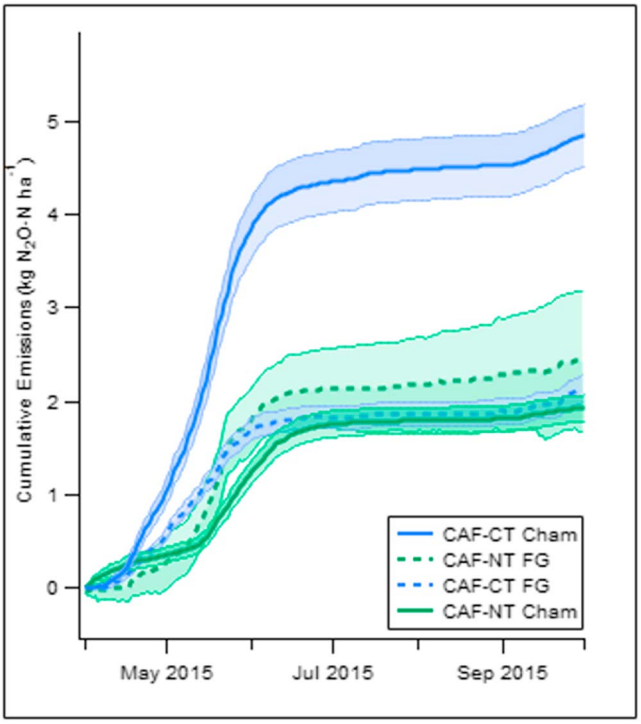

Figure 6. Cumulative N_2O emissions at the no-till site (CAF-NT, green), and the conventional till site (CAF-CT, blue) with SC (solid lines) and the FG method (dashed line). Shaded areas indicate uncertainty. For SC, uncertainty is the propagated standard error of the daily measurements. For FG, the uncertainty is the propagated random error in the 30-min measurements.

~360 m^2. Using the flux footprint parameterization (Kljun et al., 2015), we estimate that the FG systems were integrating flux signals over a cumulative area of ~2,500 m^2 (Figure 5; integrating up to the 80% flux contribution extent). There is uncertainty in footprint parameterization (cf. Heidbach et al., 2017); other footprint models (Kljun et al., 2004; Kormann & Meixner, 2001) indicate a larger footprint area (7,800 m^2 at CAF-NT and 10,000 m^2 at CAF-CT; Figure S11). Conversely, the use of the sonic anemometer height (1.91 and 2.21 m at CAF-NT and CAF-CT, respectively) rather than the geometric mean of the gradient inlet heights (1.41 and 1.53 m, respectively), could cause the footprint area to be overpredicted. Although the chamber variability also challenges the MM method requirement of a homogenous emission source over the footprint, we argue that the source should be considered homogenous at the integration scale of hundreds of square meters. Because of the large spatial variation observed in the SC results, and the greater spatial coverage of the FG technique, we will focus on the FG results when interpreting field-scale cumulative emissions at these sites.

4. Discussion

4.1. Cumulative N_2O Emissions

The cumulative emissions measured by the FG systems over the 1 April–30 September monitoring period were similar for both sites: 2.4 ± 0.7 and 2.1 ± 0.2 kg N_2O-N/ha at the no-till and conventional-till sites, respectively (Figure 6 and Table S1). The cumulative emissions measured by the SC systems over the same six-month period were 1.9 ± 0.14 and 4.8 ± 0.33 kg N_2O-N/ha at CAF-NT and CAF-CT. For the period from 1 October 2014 through 30 September 2015, the SC system observations yielded 3.9 ± 0.22 and 5.6 ± 0.34 kg N_2O-N/ha at CAF-NT and CAF-CT. The FG and SC cumulative emission magnitudes agree better at CAF-NT than CAF-CT, perhaps because of chamber location relative to the FG footprint, and the patterns of spatial variability at the two sites. The NW–SE wind pattern and hence measurement footprint of the flux gradient system has better overlap with all 16 chambers at CAF-NT than CAF-CT (Figure 5). Furthermore, at CAF-CT, there was a gradient in emission strength with SC group (Figure S13), indicating higher emissions in upslope than downslope locations. Although both sites had sloping topography (Figure S9), the chambers spanned a steeper gradient at CAF-CT than CAF-NT: 12.5% and 8% grades, respectively. Because soil moisture, chemistry, and other characteristics were not measured at the chamber sites in this study, we are not able to quantify these effects and explain the cause of the spatial pattern. Another factor that could have influenced the hierarchy in chamber emissions at CAF-CT is the potential overapplication of fertilizer. The CAF-CT site is a private, working farm, and we were not able to remove the chambers before planting and fertilization at this site, necessitating the grower to maneuver around the field trailer and other research equipment. The area avoided by the grower was hand-planted and fertilized days after, and the difference in management is visible in the satellite image (Figure 5). Similarly, the placement of the chambers relative to the spacing of the fertilizer bands was not considered in the study design. These potential departures from characterizing nominal field conditions with the SC in our study highlight the value of quantifying soil chemistry, in addition to the need for close collaboration with growers when conducting research on working agricultural fields.

The FG cumulative emissions correspond to 2.1% ± 0.6% and 1.5% ± 0.1% of the N inputs at CAF-NT and CAF-CT, respectively (Table S1), higher than the IPCC Tier 1 emission factor (EF) at CAF-NT but comparable at CAF-CT. If the 20 August fertilization in preparation for winter wheat seeding is included in the EF calculation at CAF-CT, it is 0.7% ± 0.07%, smaller than the IPCC Tier 1 EF by 33%. Evidence suggest that these EF estimates are likely conservative. First, they do not include the period of the crop year between 1 October and 1 April, a time which the SC results show that there were appreciable N_2O fluxes (Figure 2).

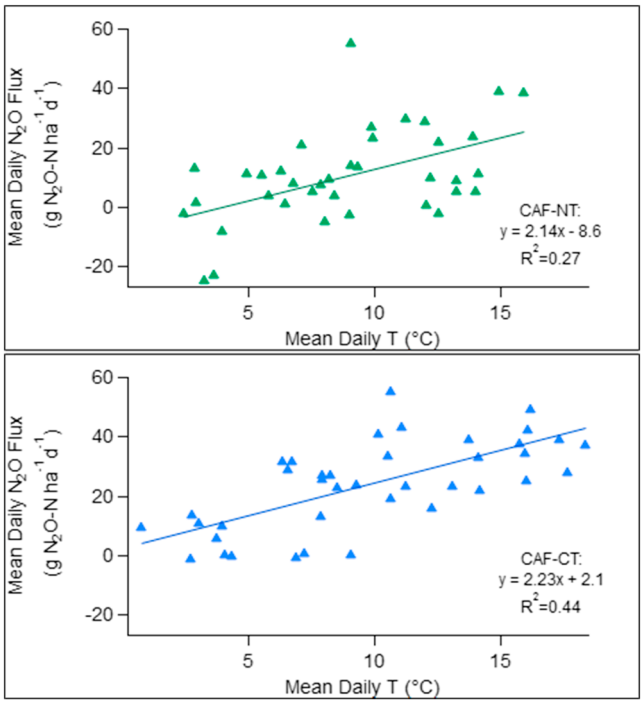

Figure 7. Linear regressions between ambient temperature and N_2O fluxes at (top) CAF-NT and (bottom) CAF-CT measured by the flux gradient (FG) method between 1 April and 11 May 2015.

Second, the comparison between K_T and K_a (Figure S10) indicated that K_T was systematically lower than K_a, suggesting that within the range of uncertainty K_T is more likely biased low than high. Lastly, many N_2O studies define the emission factor as a function of the fertilizer N input alone. Using that parameterization raises the EFs to 2.8% and 2.1% for CAF-NT and CAF-CT per the FG results.

The N_2O emission magnitudes observed in this study fall within the range of emissions reported from other systems that receive a similar amount of fertilizer N input (Figure S14). As discussed in Huang et al. (2014), there is large range in N_2O emissions reported in the literature, but the amount of N fertilizer applied tends to be the most important driver of emissions (R^2 = 0.48 in the Huang regression, R^2 = 0.37 including results from this study). Huang et al. (2014) included results from five studies that measured N_2O emissions over the growing season only (duration of three to six months). This may cause estimates of cumulative annual N_2O emissions to be biased low, as the results from this study illustrate.

4.2. Relationship Between N_2O Emissions and Environmental Variables

We observed extended periods of elevated N_2O emissions following spring rains. Rain can flush existing N_2O from soil pores (Huang et al., 2014), and the added moisture can create anaerobic microsites in soil pores that are hot spots for denitrification, leading to elevated N_2O production and emission (Pihlatie et al., 2005). The emission events following the 12–16 May rainfall at both sites lasted for approximately a month (Figure 2), indicating that the rainfall lead to enhanced production of N_2O at these sites. Conversely, the one-day spike in emissions after the 10 July rainfall event was likely a physical flush of N_2O-rich air from the soil pore space.

Both N_2O emission "spikes" of approximately one day and "pulses" lasting weeks (coined by Cai et al. (2013)) have been observed in other N_2O monitoring studies. Studies have reported emission spikes following rainfall lasting less than one day in agroecosystems (Barton et al., 2011; Glenn et al., 2012; Huang et al., 2014), spikes lasting two to six days following fertilization (Jones et al., 2011), elevated N_2O emissions lasting on the order of two weeks following fertilization and rainfall (Cai et al., 2013; Tallec et al., 2019; Zhou et al., 2013), and emission pulses lasting two months in grassland systems following tillage (Cowan et al., 2016). In the context of these prior studies, the monthlong periods of sustained elevated emissions observed at both cropland sites in this study are important for monitoring, understanding, and predicting future N_2O emissions from these systems.

Both the conventional tillage and no-tillage site N_2O emissions responded similarly to temperature. Linear regressions between mean daily temperature and mean daily N_2O fluxes from 1 April to 11 May 2015 measured by the FG system for each site have similar slopes (2.14 and 2.23 at CAF-NT and CAF-CT, respectively; Figure 7), indicating that emissions respond similarly to changes in temperature, absent other environmental drivers. We truncated the data set at 11 May 2015 to minimize the influence of the 12–15 May precipitation event (affecting soil moisture) on the measured N_2O fluxes.

While CO_2 respiration is not a direct driver of N_2O production and emission, the same environmental conditions (e.g., soil temperature, moisture, and microbial activity) can have similar influences on the production and emission of both CO_2 and N_2O (Knox et al., 2016; Morin et al., 2014). Linear regressions between N_2O emission and CO_2 respiration in the winter (1 October 2014 to 1 March 2015) have similar slopes (0.19 and 0.25 at CAF-NT and CAF-CT, respectively), but the relationship is stronger at CAF-NT than CAF-CT, with an adjusted R^2 value of 0.55 versus 0.26 (Figure S15). Figures S16–S20 illustrate how the relationships between N_2O and CO_2 emissions break down by individual chamber and by winter and growing season time periods.

4.3. Implications of N_2O Emission Results for Overall N and GHG Budgets

The emission rates observed in this study are comparable to literature values (Huang et al., 2014; Figure S14). However, we are interested in increasing our knowledge of local N_2O emission behavior. Prior to this study, there was only one published article reporting direct N_2O emission measurements in the iPNW region (Cochran et al., 1981), which found that <0.1% of fertilizer N was emitted as N_2O. A more recent study used a process-based model to simulate N_2O emissions for several representative areas and management practices in the iPNW, including scenarios co-located with the CAF-NT and CAF-CT sites (Stöckle et al., 2012). The simulation results found these systems were sources of N_2O at a rate of 0.72 to 0.98 kg N_2O-N ha^{-1} yr^{-1}, and had emission factors of 0.71% to 1.1% of applied fertilizer N. These simulation study results agree reasonably well with the IPCC Tier 1 estimates, and with the conservative EF calculated for CAF-CT but are lower than the upper EF estimates of this study by a factor of 2.

The difference between the N_2O emission results from this study and previous best estimates has important implications when propagated to the GHG budget of the systems. Typical rates of increase in soil organic carbon after converting to no-tillage management for continuous cropping systems have been reported at 25 g C m^{-2} yr^{-1} (West & Post, 2002), 20 g C m^{-2} yr^{-1} (Brown & Huggins, 2012), and 16–23 g C m^{-2} yr^{-1} (Stöckle et al., 2012). The global warming potential of N_2O emissions characterized in this study is on the high end of typical soil C uptake, equivalent to 27 ± 8 g C m^{-2} yr^{-1} per the FG results at CAF-NT, and 24 ± 2 g C m^{-2} yr^{-1} per the FG results at CAF-CT. The rate of C uptake in soils after converting to no-till lasts 15–20 years with diminishing returns, while N_2O emissions persist over time.

5. Summary and Conclusions

In this study, automated SC and the FG technique were used to monitor N_2O emissions over two canola fields under different tillage regimes in the inland Pacific Northwest. An array of 16 automated static chambers was operated at each site over the entire 2015 crop year, while results from the FG measurements were available from 1 April to 30 September 2015. Maximum emissions were observed at both sites in response to multiple rain events following fertilization, and the elevated emissions lasted on the order of one month at both sites. Ambient temperature as well as CO_2 respiration were positively correlated with N_2O emissions at both sites. The FG results indicated that total emissions were 2.4 ± 0.7 and 2.1 ± 0.2 kg N_2O-N/ha, respectively, from the no-till and conventional till sites. This translates to N_2O emission factors of 2.1% and 1.5% respectively, likely conservative estimates due to the six-month duration of the measurements and other biases discussed in section 4.1.

The results of this study highlight the limitations inherent in characterizing field-scale fluxes with SC point measurements. We reemphasize the recommendation of other groups (cf. Jones et al., 2011; Tallec et al., 2019): rely on micrometeorological methods or other methods that integrate over larger spatial scales to answer questions about field-scale processes (i.e., total cumulative N_2O emissions) and use SC to validate the observed temporal patterns. The SC measurements in tandem with co-located measurements of environmental variables can answer questions about biophysical drivers of N_2O production and emission useful for parameterizing models. There are plans to continue monitoring N_2O fluxes at paired conventional tillage and no-tillage sites as part of the USDA Long-Term Agroecosystem Research program at Cook Agronomy Farm, and this future work should include measurements of soil texture, moisture, mineral N, and other factors that affect N_2O production and emission co-located with SC to aid in the interpretation and upscaling of both SC and FG results. Identifying the N_2O production pathways and parameterizing N_2O:N_x product ratios for these systems should be prioritized to determine the gaseous loss term of the N budget (cf. Butterbach-Bahl et al., 2013; Wrage et al., 2001). If denitrification is a dominant production pathway, total losses of N as $N_2O + N_2$ could be an agronomically important part of the N budget in this region. For systems such as the ones in this study with high spatial heterogeneity, combining measurements and process-based models may be the best strategy to estimate field-scale and regional emissions of N_2O. Future SC studies investigating drivers could be used to improve the parameterization of N_2O dynamics in process-based models such as CropSyst (Stöckle et al., 2003), and FG or eddy covariance field-scale results could be used to constrain the cumulative emissions.

Despite the limitations of this study, the consistent findings at both sites that these agronomic fields are a larger source of N_2O than previously assumed based on the IPCC methodology and previous site-specific best estimates, and that the N_2O emissions likely outweigh C storage in the soils, showing the importance of management in mitigating N_2O emissions along with conserving and building soil organic carbon in the iPNW.

Acknowledgments
This study was funded through the "Regional Approaches to Climate Change for Pacific Northwest Agriculture" (REACCH-PNA) project, USDA NIFA award 2011-68002-30191. The assistance of Pavlo Rudenko and William Riley Devine in designing and maintaining the power systems at the monitoring sites and that of Ian Leslie in analyzing site topography is gratefully acknowledged. S.W. was also supported through the NSF IGERT "Nitrogen Systems: Policy-oriented Integrated Research and Education," and through the EPA STAR fellowship. This publication was developed under STAR Fellowship Assistance agreement FP-91770001-0 awarded by the U.S. Environmental Protection Agency (EPA). WSU Pullman and the Cook Agronomy Farm are located on the ancestral homelands of the Palus people and the ceded lands of the Nez Perce Tribe. This document has been reviewed in accordance with U.S. Environmental Protection Agency policy and approved for external publication. The views expressed in this article are those of the authors and do not necessarily represent the opinions or policies of the U.S. Environmental Protection Agency. Any mention of trade names or commercial products does not constitute endorsement or recommendation for use. This publication does not represent the views of the New York City. The data supporting the conclusions of this publication and the data processing scripts may be found online: https://osf.io/bc6rm/?view_only=724f5e6a4e004d02a008ae74724cfa5e.

References

Bai, M., Suter, H., Lam, S. K., Flesch, T. K., & Chen, D. L. (2019). Comparison of slant open-586 path flux gradient and static closed chamber techniques to measure soil N_2O emissions, 587. *Atmospheric Measurement Techniques*, *12*(2), 1095–1102. https://doi.org/10.5194/amt-12-1095-5882019

Baldocchi, D., Guenther, A., Harley, P., Klinger, L., Zimmerman, P., Lamb, B., & Westberg, H. (1995). The fluxes and air chemistry of isoprene above a deciduous hardwood forest. *Philosophical Transactions of the Royal Society A-Mathematical Physical and Engineering Sciences*, *351*(1696), 279–296. https://doi.org/10.1098/rsta.1995.0034

Barton, L., Butterbach-Bahl, K., Kiese, R., & Murphy, D. V. (2011). Nitrous oxide fluxes from a grain-legume crop (narrow-leafed lupin) grown in a semiarid climate. *Global Change Biology*, *17*(2), 1153–1166. https://doi.org/10.1111/j.1365-2486.2010.02260.x

Barton, L., Wolf, B., Rowlings, D., Scheer, C., Kiese, R., Grace, P., et al. (2015). Sampling frequency affects estimates of annual nitrous oxide fluxes. *Science Report*, *5*(1), 15912. https://doi.org/10.1038/srep15912

Bista, P., Machado, S., Ghimire, R., Yorgey, G., and Wysocki, D. (2017). Conservation tillage 601 systems. Chapter 3 in Advances in dryland farming in the inland Pacific Northwest. 602 http://pubs.cahnrs.wsu.edu/publications/pubs/em108/

Brown, S. E., & Wagner-Riddle, C. (2017). Assessment of random errors in multi-plot nitrous oxide flux gradient measurements. *Agricultural and Forest Meteorology*, *242*, 10–20. https://doi.org/10.1016/j.agrformet.2017.04.005

Brown, T. T., & Huggins, D. R. (2012). Soil carbon sequestration in the dryland cropping region of the Pacific Northwest. *Journal of Soil and Water Conservation*, *67*(5), 406–415. https://doi.org/10.2489/jswc.67.5.406

Businger, J. A., Wyngaard, J. C., Izumi, Y., & Bradley, E. F. (1971). Flux–profile relationships in the atmospheric surface layer. *Journal of the Atmospheric Sciences*, *28*(2), 181–189. https://doi.org/10.1175/1520-0469(1971)028<0181:FPRITA>2.0.CO;2

Butterbach-Bahl, K., Baggs, E. M., Dannenmann, M., Kiese, R., & Zechmeister-Boltenstern, S. (2013). Nitrous oxide emissions from soils: How well do we understand the processes and their controls? *Philosophical Transactions of the Royal Society B-Biological Sciences*, *368*(1621). https://doi.org/10.1098/rstb.2013.0122

Cai, Y., Ding, W., & Luo, J. (2013). Nitrous oxide emissions from Chinese maize–wheat rotation systems: A 3-year field measurement. *Atmospheric Environment*, *65*, 112–122. https://doi.org/10.1016/j.atmosenv.2012.10.038

Chi, J., Maureira, F., Waldo, S., Pressley, S. N., Stöckle, C. O., O'Keeffe, P. T., et al. (2017). Carbon and water budgets in multiple wheat-based cropping systems in the inland Pacific Northwest US: Comparison of CropSyst simulations with eddy covariance measurements. *Frontiers in Ecology and Evolution*, *5*. https://doi.org/10.3389/fevo.2017.00050

Chi, J., Waldo, S., Pressley, S., O'Keeffe, P., Huggins, D., Stöckle, C., et al. (2016). Assessing carbon and water dynamics of no-till and conventional tillage cropping systems in the inland Pacific Northwest US using the eddy covariance method. *Agricultural and Forest Meteorology*, *218-219*, 37–49. https://doi.org/10.1016/j.agrformet.2015.11.019

Christensen, S., Ambus, P., Arah, J. R. M., Clayton, H., Galle, B., Griffith, D. W. T., et al. (1996). Nitrous oxide emission from an agricultural field: Comparison 628 between measurements by flux chamber and micrometerological techniques. *Atmospheric 629 Environment*, *30*(24), 4183–4190. https://doi.org/10.1016/1352-2310(96)00145-8

Cochran, V. L., Elliott, L. F., & Papendick, R. I. (1981). Nitrous-oxide emissions from a fallow field fertilized with anhydrous ammonia. *Soil Science Society of America Journal*, *45*(2), 307–310. https://doi.org/10.2136/sssaj1981.03615995004500020016x

Cowan, N. J., Levy, P. E., Famulari, D., Anderson, M., Drewer, J., Carozzi, M., et al. (2016). The influence of tillage on N_2O fluxes from an intensively managed grazed grassland in Scotland. *Biogeosciences*, *13*(16), 4811–4821. https://doi.org/10.5194/bg-13-4811-2016

Denmead, O. T., Macdonald, B. C. T., Bryant, G., Naylor, T., Wilson, S., Griffith, D. W. T., et al. (2010). Emissions of methane and nitrous 638 oxide from Australian sugarcane soils. *Agricultural and Forest Meteorology*, *150*(6), 748–756. https://doi.org/10.1016/j.agrformet.2009.06.018

Dunn, A. L., Wofsy, S. C., & Bright, A. v. H. (2009). Landscape heterogeneity, soil climate, and carbon exchange in a boreal black spruce forest. *Ecological Applications*, *19*(2), 495–504. https://doi.org/10.1890/07-0771.1

Dyer, A. J., & Hicks, B. B. (1970). Flux–gradient relationships in the constant flux layer. *Quarterly Journal of the Royal Meteorological Society*, *96*(410), 715–721. https://doi.org/10.1002/qj.49709641012

Falge, E., Baldocchi, D., Olson, R., Anthoni, P., Aubinet, M., Bernhofer, C., et al. (2001). Gap filling strategies for defensible annual sums of net ecosystem exchange. *Agricultural and Forest Meteorology*, *107*(1), 43–69. https://doi.org/10.1016/S0168-1923(00)00225-2

Finkelstein, P. L., & Sims, P. F. (2001). Sampling error in eddy correlation flux measurements. *Journal of Geophysical Research*, *106*(D4), 3503–3509. https://doi.org/10.1029/2000JD900731

Flesch, T. K., Baron, V. S., Wilson, J. D., Basarab, J. A., Desjardins, R. L., Worth, D., & Lemke, R. L. (2018). Micrometeorological measurements reveal large nitrous oxide losses 653 during spring thaw in Alberta. *Atmosphere*, *9*(4). https://doi.org/10.3390/atmos9040128

Foken, T., & Wichura, B. (1996). Tools for quality assessment of surface-based flux measurements. *Agricultural and Forest Meteorology*, *78*(1-2), 83–105. https://doi.org/10.1016/0168-1923(95)02248-1

Galloway, J. N., Townsend, A. R., Erisman, J. W., Bekunda, M., Cai, Z., Freney, J. R., et al. (2008). Transformation of the nitrogen cycle: Recent trends, questions, and potential solutions. *Science*, *320*(5878), 889–892. https://doi.org/10.1126/science.1136674

Glenn, A. J., Tenuta, M., Amiro, B. D., Maas, S. E., & Wagner-Riddle, C. (2012). Nitrous oxide emissions from an annual crop rotation on poorly drained soil on the Canadian Prairies. *Agricultural and Forest Meteorology*, *166-167*, 41–49. https://doi.org/10.1016/j.agrformet.2012.06.015

Goldstein, A. H., Fan, S. M., Goulden, M. L., Munger, J. W., & Wofsy, S. C. (1996). Emissions of ethene, propene, and 1-butene by a mid-latitude forest. *Journal of Geophysical Research*, *101*(D4), 9149–9157. https://doi.org/10.1029/96jd00334

Groffman, P. M., Altabet, M. A., Böhlke, J. K., Butterbach-Bahl, K., David, M. B., Firestone, M. K., et al. (2006). Methods for measuring denitrification: Diverse approaches to a difficult problem. *Ecological Applications*, *16*(6), 2091–2122. https://doi.org/10.1890/1051-0761(2006)016[2091:mfmdda]2.0.co;2

Groffman, P. M., Brumme, R., Butterbach-Bahl, K., Dobbie, K. E., Mosier, A. R., Ojima, D., et al. (2000). Evaluating annual nitrous oxide fluxes at the ecosystem scale. *Global Biogeochemical Cycles*, *14*(4), 1061–1070. https://doi.org/10.1029/1999GB001227

Heidbach, K., Schmidt, H. P., & Mauder, M. (2017). Experimental evaluation of flux footprint models. *Agricultural and Forest Meteorology*, *246*, 142–153. https://doi.org/10.1016/j.agrformet.2017.06.008

Huang, H., Wang, J., Hui, D., Miller, D. R., Bhattarai, S., Dennis, S., et al. (2014). Nitrous oxide emissions from a commercial cornfield (*Zea mays*) measured using the eddy covariance technique. *Atmospheric Chemistry and Physics*, *14*(23), 12,839–12,854. https://doi.org/10.5194/acp-14-12839-2014

IPCC. (2006). 2006 IPCC guidelines for national greenhouse gas inventories, prepared by the National Greenhouse Gas Inventories Programme. Retrieved from Japan: www.ipcc-nggip.iges.or.jp/public/2006gl/

Jones, S. K., Famulari, D., Di Marco, C. F., Nemitz, E., Skiba, U. M., Rees, R. M., & Sutton, M. A. (2011). Nitrous oxide emissions from managed grassland: a comparison of eddy covariance and static chamber measurements. *Atmospheric Measurement Techniques*, *4*(10), 2179–2194. https://doi.org/10.5194/amt-4-2179-2011

Kljun, N., Calanca, P., Rotach, M. W., & Schmid, H. P. (2004). A simple parameterisation for flux footprint predictions. *Boundary-Layer Meteorology*, *112*(3), 503–523. https://doi.org/10.1023/B:BOUN.0000030653.71031.96

Kljun, N., Calanca, P., Rotach, M. W., & Schmid, H. P. (2015). A simple two-dimensional parameterisation for flux footprint prediction (FFP). *Geoscientific Model Development*, *8*(11), 3695–3713. https://doi.org/10.5194/gmd-8-3695-2015

Knox, S. H., Matthes, J. H., Sturtevant, C., Oikawa, P. Y., Verfaillie, J., & Baldocchi, D. (2016). Biophysical controls on interannual variability in ecosystem-scale CO_2 and CH_4 exchange in a California rice paddy. *Journal of Geophysical Research: Biogeosciences*, *121*, 978–1001. https://doi.org/10.1002/2015JG003247

Kormann, R., & Meixner, F. X. (2001). An analytical footprint model for non-neutral stratification. *Boundary-Layer Meteorology*, *99*(2), 207–224. https://doi.org/10.1023/A:1018991015119

Kostyanovsky, K. I., Huggins, D. R., Stöckle, C. O., Waldo, S., & Lamb, B. (2017). Developing a flow through chamber system for automated measurements of soil N_2O and CO_2 emissions. *Measurement*, *113*, 172–180. https://doi.org/10.1016/j.measurement.2017.05.040

Kroon, P. S., Hensen, A., Jonker, H. J. J., Ouwersloot, H. G., Vermeulen, A. T., & Bosveld, F. C. (2010). Uncertainties in eddy covariance flux measurements assessed from CH_4 and N_2O observations. *Agricultural and Forest Meteorology*, *150*(6), 806–816. https://doi.org/10.1016/j.agrformet.2009.08.008

Laville, P., Jambert, C., Cellier, P., & Delmas, R. (1999). Nitrous oxide fluxes from a fertilised maize crop using micrometeorological and chamber methods. *Agricultural and Forest Meteorology*, *96*(1–3), 19–38. https://doi.org/10.1016/S0168-1923(99)00054-4

Liu, H. P., & Foken, T. (2001). A modified Bowen ratio method to determine sensible and latent heat fluxes. *Meteorologische Zeitschrift*, *10*(1), 71–80. https://doi.org/10.1127/0941-2948/2001/0010-0071

Loescher, H. W., Law, B. E., Mahrt, L., Hollinger, D. Y., Campbell, J., & Wofsy, S. C. (2006). Uncertainties in, and interpretation of, carbon flux estimates using the eddy covariance technique. *Journal of Geophysical Research*, *111*, D21S90. https://doi.org/10.1029/2005JD006932

Lugato, E., Leip, A., & Jones, A. (2018). Mitigation potential of soil carbon management overestimated by neglecting N_2O emissions. *Nature Climate Change*, *8*(3), 219–223. https://doi.org/10.1038/s41558-018-0087-z

Mason, C. W., Stoof, C. R., Richards, B. K., Das, S., Goodale, C. L., & Steenhuis, T. S. (2017). Hotspots of nitrous oxide emission in fertilized and unfertilized perennial grasses. *Soil Science Society of America Journal*, *81*(3), 450. https://doi.org/10.2136/sssaj2016.08.0249

McClain, M. E., Boyer, E. W., Dent, C. L., Gergel, S. E., Grimm, N. B., Groffman, P. M., et al. (2003). Biogeochemical hot spots and hot moments at the interface of terrestrial and aquatic ecosystems. *Ecosystems*, *6*(4), 301–312. https://doi.org/10.1007/s10021-003-0161-9

McDaniel, M. D., Simpson, R. R., Malone, B. P., McBratney, A. B., Minasny, B., & Adams, M. A. (2017). Quantifying and predicting spatio-temporal variability of soil CH_4 and N_2O fluxes from a seemingly homogeneous Australian agricultural field. *Agriculture, Ecosystems & Environment*, *240*, 182–193. https://doi.org/10.1016/j.agee.2017.02.017

Meredith, L. K., Commane, R., Munger, J. W., Dunn, A., Tang, J., Wofsy, S. C., & Prinn, R. G. (2014). Ecosystem fluxes of hydrogen: A comparison of flux-gradient methods. *Atmospheric Measurement Techniques*, *7*(9), 2787–2805. https://doi.org/10.5194/amt-7-2787-2014

Meyers, T. P., Hall, M. E., Lindberg, S. E., & Kim, K. (1996). Use of the modified Bowen-ratio technique to measure fluxes of trace gases. *Atmospheric Environment*, *30*(19), 3321–3329. https://doi.org/10.1016/1352-2310(96)00082-9

Millar, N., Urrea, A., Kahmark, K., Shcherbak, I., Robertson, G. P., & Ortiz-Monasterio, I. (2018). Nitrous oxide (N_2O) flux responds exponentially to nitrogen fertilizer in irrigated wheat in the Yaqui Valley, Mexico. *Agriculture, Ecosystems & Environment*, *261*, 125–132. https://doi.org/10.1016/j.agee.2018.04.003

Moffat, A. M., Papale, D., Reichstein, M., Hollinger, D. Y., Richardson, A. D., Barr, A. G., et al. (2007). Comprehensive comparison of gap-filling techniques for eddy covariance net carbon fluxes. *Agricultural and Forest Meteorology*, *147*(3-4), 209–232. https://doi.org/10.1016/j.agrformet.2007.08.011

Molodovskaya, M., Singurindy, O., Richards, B. K., Warland, J., Johnson, M. S., & Steenhuis, T. S. (2012). Temporal variability of nitrous oxide from fertilized croplands: Hot moment analysis. *Soil Science Society of America Journal*, *76*(5), 1728. https://doi.org/10.2136/sssaj2012.0039

Morin, T. H., Bohrer, G., Frasson, R. P. D. M., Naor-Azreli, L., Mesi, S., Stefanik, K. C., & Schäfer, K. V. R. (2014). Environmental drivers of methane fluxes from an urban temperate wetland park. *Journal of Geophysical Research: Biogeosciences*, *119*, 2188–2208. https://doi.org/10.1002/2014JG002750

Myhre, G., Shindell, D., Bréon, F.-M., Collins, W., Fuglestvedt, J., Huang, J., et al. (2013). Anthropogenic and natural radiative forcing. In Climate change 2013: The physical science basis. Contribution of Working Group I to the Fifth Assessment Report of the Intergovernmental Panel on Climate Change. Cambridge, UK and New York.

Neftel, A., Ammann, C., Fischer, C., Spirig, C., Conen, F., Emmenegger, L., et al. (2010). N2O exchange over managed grassland: Application of a quantum cascade laser spectrometer for micrometeorological flux measurements. *Agricultural and Forest Meteorology*, *150*(6), 775–785. https://doi.org/10.1016/j.agrformet.2009.07.013

Nicolini, G., Castaldi, S., Fratini, G., & Valentini, R. (2013). A literature overview of micrometeorological CH4 and N2O flux measurements in terrestrial ecosystems. *Atmospheric Environment*, *81*, 311–319. https://doi.org/10.1016/j.atmosenv.2013.09.030

Norman, J. M., Kucharik, C. J., Gower, S. T., Baldocchi, D. D., Crill, P. M., Rayment, M., et al. (1997). A comparison of six methods for measuring soil-764 surface carbon dioxide fluxes. *Journal of Geophysical Research*, *102*(D24), 28,771–28,777. https://doi.org/10.1029/97JD01440

Pattey, E., Edwards, G., Strachan, I. B., Desjardins, R. L., Kaharabata, S., & Riddle, C. W. (2006). Towards standards for measuring greenhouse gas fluxes from agricultural fields using instrumented towers. *Canadian Journal of Soil Science*, *86*(3), 373–400. https://doi.org/10.4141/S05-100

Phillips, F. A., Leuning, R., Baigenta, R., Kelly, K. B., & Denmead, O. T. (2007). Nitrous oxide flux measurements from an intensively managed irrigated pasture using micrometeorological techniques. *Agricultural and Forest Meteorology*, *143*(1-2), 92–105. https://doi.org/10.1016/j.agrformet.2006.11.011

Pihlatie, M., Rinne, J., Ambus, P., Pilegaard, K., Dorsey, J. R., Rannik, U., et al. (2005). Nitrous oxide emissions from a beech forest floor measured by eddy covariance and soil enclosure techniques. *Biogeosciences*, *2*(4), 377–387. https://doi.org/10.5194/bg-2-377-2005

Ravishankara, A. R., Daniel, J. S., & Portmann, R. W. (2009). Nitrous oxide (N_2O): The dominant ozone-depleting substance emitted in the 21st century. *Science*, *326*(5949), 123–125. https://doi.org/10.1126/science.1176985

Reay, D. S., Davidson, E. A., Smith, K. A., Smith, P., Melillo, J. M., Dentener, F., & Crutzen, P. J. (2012). Global agriculture and nitrous oxide emissions. *Nature Climate Change*, *2*(6), 410–416. https://doi.org/10.1038/Nclimate1458

Shcherbak, I., Millar, N., & Robertson, G. P. (2014). Global metaanalysis of the nonlinear response of soil nitrous oxide (N_2O) emissions to fertilizer nitrogen. *Proceedings of the National Academy of Sciences of the United States of America*, *111*(25), 9199–9204. https://doi.org/10.1073/pnas.1322434111

Shrewsbury, L. H., Smith, J. L., Huggins, D. R., Carpenter-Boggs, L., & Reardon, C. L. (2016). Denitrifier abundance has a greater influence on denitrification rates at larger landscape scales but is a lesser driver than environmental variables. *Soil Biology and Biochemistry*, *103*, 221–231.

Singh, A., Maichle, R., & Lee, S. E. (2006). On the computation of a 95% upper confidence limit of the unknown population mean based upon data sets with below detection limit observations. Retrieved from https://nepis.epa.gov.

Stöckle, C., Higgins, S., Kemanian, A., Nelson, R., Huggins, D., Marcos, J., & Collins, H. (2012). Carbon storage and nitrous oxide emissions of cropping systems in eastern Washington: A simulation study. *Journal of Soil and Water Conservation*, *67*(5), 365–377. https://doi.org/10.2489/jswc.67.5.365

Stöckle, C. O., Donatelli, M., & Nelson, R. (2003). CropSyst, a cropping systems simulation model. *European Journal of Agronomy*, *18*(3-4), 289–307. https://doi.org/10.1016/S1161-0301(02)00109-0

Syakila, A., & Kroeze, C. (2012). The global nitrous oxide budget revisited. *Greenhouse gas measurement and management*, *1*(1), 9.

Tallec, T., Brut, A., Joly, L., Dumelié, N., Serça, D., Mordelet, P., et al. (2019). N_2O flux measurements over an irrigated maize crop: A comparison of three methods. *Agricultural and Forest Meteorology*, *264*, 56–72. https://doi.org/10.1016/j.agrformet.2018.09.017

USEPA. (2017). Inventory of U.S. greenhouse gas emissions and sinks: 1990–2015.

Wagner-Riddle, C., Furon, A., MClaughlin, N. L., Lee, I., Barbeau, J., Jayasundara, S., et al. (2007). Intensive measurement of nitrous oxide emissions from a corn?soybean?wheat rotation under two contrasting management systems over 5 years. *Global Change Biology*, *13*(8), 1722–1736. https://doi.org/10.1111/j.1365-2486.2007.01388.x

Waldo, S., Chi, J., Pressley, S. N., O'Keeffe, P., Pan, W. L., Brooks, E. S., et al. (2016). Assessing carbon dynamics at high and low rainfall agricultural sites in the inland Pacific Northwest US using the eddy covariance method. *Agricultural and Forest Meteorology*, *218-219*, 25–36. https://doi.org/10.1016/j.agrformet.2015.11.018

Wang, K., Zheng, X., Pihlatie, M., & Vesala, T. (2013). Comparison between static chamber and tunable diode laser-based eddy covariance techniques for measuring nitrous oxide fluxes from a cotton field. *Agricultural and Forest Meteorology*, *171-172*, 9–19. https://doi.org/10.1016/j.agrformet.2012.11.009

West, T. O., & Post, W. M. (2002). Soil organic carbon sequestration rates by tillage and crop rotation: A global data analysis. *Soil Science Society of America Journal*, *66*(6), 1930–1946. https://doi.org/10.2136/sssaj2002.1930

Wrage, N., Velthof, G. L., van Beusichem, M. L., & Oenema, O. (2001). Role of nitrifier denitrification in the production of nitrous oxide. *Soil Biology & Biochemistry*, *33*, 9.

Zhou, M. H., Zhu, B., Butterbach-Bahl, K., Zheng, X. H., Wang, T., & Wang, Y. Q. (2013). Nitrous oxide emissions and nitrate leaching from a rain-fed wheat-maize rotation in the Sichuan Basin, China. *Plant and Soil*, *362*(1-2), 149–159. https://doi.org/10.1007/s11104-012-1269-5